Multi-dimentional upwind schemes for the Euler Equations on unstructured grids

Mounir Aksas m_aksas@hotmail.com
LPEA, Department of Physics, Faculty of Sciences
University of Batna
05000 Batna, Algeria

Abdelmouman H. Benmachiche h_benmach@yahoo.com
Department of Mechanics, Faculty of Engineering
University of Biskra
07000 Biskra, Algeria

ABSTRACT

In the last few years, upwind methods have become very popular in the modeling of advection dominated flows and in particular those which contain strong discontinuities. For more than a decade, these methods have been used successfully to solve numerically the one-dimensional Euler equations. Fluctuation distribution has been recently introduced as an alternative to conventional upwinding. In contrast to standard upwinding the fluctuation distribution approach extends naturally to multidimensional flow without requiring any splitting along coordinate directions. The technique uses a narrow-stencil, local, piecewise linear reconstruction of the flow field solution. The flow field is updated in time by propagating a subset of eigenmodes of the convective operator. Different choices of the eigenmode subset lead to different fluctuation distribution schemes.

In this paper, schemes for approximating steady solution to the two dimensional of the inviscid fluid equations on unstructured triangular grids are presented, also an analysis of fluctuation splitting schemes applied to scalar advection equations has been performed. Wave models based on Roe's simple wave decomposition have been further developed and tested, providing an exact solution to the linearized equations, and decomposes the flux difference at the interface into a set of simple waves, all aligned with the grid face.

In this work, the presented model of fluctuation splitting N combined with Roe wave models implemented in our own Code written in C++ reached the stage where they can be used reliably to achieve maximal computational efficiency to practical steady state problems in aerodynamics (Supersonic oblique shock reflection, Flow in a channel with a Bump, Symmetric Constricted channel flows, flow around NACA 0012 aerofoil, flows in a turbine-blade cascade VKI LS-59).

Keywords: CFD, upwind, fluctuation, Euler equation, Roe, unstructured triangular meshes.

1. INTRODUCTION

The equations describing inviscid and non-heat conducting flow are the Euler equations, form a hyperbolic system of conservation laws for mass, momentum and energy, in which information travels along particular directions called characteristics.
The development of numerical methods for solving the multidimensional Euler equations with improved shock-capturing properties has been a very important research topic in CFD.

Over the past decade, there has been a considerable interest in developing multidimensional upwind methods for the Euler equations, in the goal to remove the limitations of classical upwind methods based on one dimensional Riemann problem. The difference between this and most other finite volume methods used to solve systems of conservation laws is that it involves the decomposition of the governing equations into simple components, each of which is treated individually in a genuinely multidimensional manner [12]. This avoids the misinterpretation of certain flow features, which is inherent in many of the traditional techniques used to extend upwind finite volume schemes to higher dimensions, whilst retaining the shock capturing capabilities that have made upwinding so effective in one dimension [11].

Actually multidimensional upwinding methods developed by Sidilkover, initially based on structured finite-volume grids but extended to unstructured cell-vertex grids, have been unified with the fluctuation splitting schemes [9,12]. The formulation of Sidilkover utilizes symmetric limiting functions, for which any existing one dimensional limiting method can be substituted, given that an elegant framework which surround a large variety of schemes [10].

In this work we decompose the Euler system into a set of six simple wave equations [7,8]. The resulting scalar equations are solved using one of the newly developed multidimensional fluctuation splitting schemes, which distribute the residual in an upwind fashion over a compact cell-vertex stencil [5]. The schema originally proposed by Roe [7] and further developed in [14], provided a very robust method for solving the Euler equations when combined with the fluctuation splitting N scheme.

2. METHODOLOGY

2.1 Governing Equations

The continuity, momentum and energy equations, governing the unsteady two-dimensional flow of an inviscid fluid (called the Euler equations) are written in conservative form in a cartesian coordinate system as follows:

$$\frac{\partial U}{\partial t}+\frac{\partial F}{\partial x}+\frac{\partial G}{\partial y}=0 \qquad (1)$$

where U is a state vector of dependent variables and F and G are the flux vectors in the x and y directions, and are given by:

$$U=\begin{bmatrix}\rho\\ \rho u\\ \rho v\\ \rho E\end{bmatrix},\ F=\begin{bmatrix}\rho u\\ \rho u^2+p\\ \rho uv\\ \rho uH\end{bmatrix},\ G=\begin{bmatrix}\rho v\\ \rho uv\\ \rho v^2+p\\ \rho vH\end{bmatrix} \qquad (2)$$

Assuming that the fluid is an ideal gas thermally and calorically and, given the definition of total enthalpy H.

$$H=E+p/\rho \qquad (3)$$

The pressure p can then be written as :

$$p=(\gamma-1)\rho\left[E-\frac{1}{2}\left(u^2+v^2\right)\right] \qquad (4)$$

where γ is the ratio of specific heats.

2.2 Fluctuation distribution scheme

Perhaps the most-widely used numerical method to solve the above system is the finite-volume technique coupled with a time-advancement scheme that is based upon some known, physical solution. For 1D flow the solution to the Riemann problem is widely used. The solution is used an "upwind" manner in which flow field information is propagated in a physically meaningful direction. For multidimensional flow there is no readily available solution to the Riemann problem of constant flow field variables on each computational cell. In the absence of a "multidimensional Riemann solver" [8] the 1D Riemann problem solution is often applied independently on each spatial dimension, a procedure widely known as splitting. Splitting however, has no physical justification. Roe proposed some time ago [8], [9] to move away from the piecewise constant representation implicit in the Riemann problem in looking for a means by which to include true, physical multidimensional effects in a flow solver. Roe suggested a piecewise linear representation of the flow field. The natural domain discretization is in this case into triangles for 2D. The quasi-linear form of the Euler equations is:

$$U_t + A^U U_x + B^U U_y = U_t + \vec{F}^U . \nabla U = 0 \qquad (5)$$

Over a computational cell (i.e. a triangle) the gradient is constant in the piecewise linear approximation. It may be expanded in a basis formed by eigenmodes r_k of the Jacobian $\vec{\mathrm{F}}^U$ projected along some direction $\vec{\mu}_k$, i.e. of the matrix $\left(\vec{\mathrm{F}}^U , \vec{\mu}_k \right)$,

$$\vec{\nabla} U = \sum_k \alpha_k \vec{\mu}_k \, r_k \qquad (6)$$

Integration of (5) over a triangle *T* leads to :

$$\begin{aligned} \iint_T U_t ds &= -\iint_T \sum_k \alpha_k \left(\vec{\mathrm{F}}^U . \vec{\mu}_k \right) . r_k \, ds \\ &= -\iint_T \sum_k \alpha_k \lambda_k . r_k \, ds = -\Phi^T \end{aligned} \qquad (7)$$

where λ_k are the eignvalues from $\left(\vec{\mathrm{F}}^U . \vec{\mu}_k \right) . r_k = \lambda_k . r_k$.

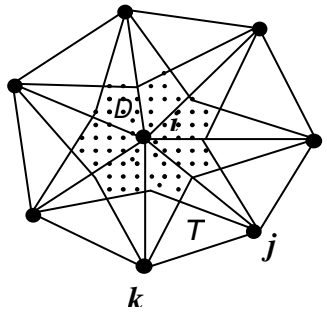

FIGURE 1: The median dual cell around a grid node, *i. "T"* is a typical triangle contains nodes *i, j, k.*

The quantity Φ^T is referred as the fluctuation in cell *T*. In general λ_k , r_k depend on U which is modified during a time step. We may however consider a constant value (denoted by an overbar) for λ_k , r_k over the cell *T* over a time step.

$$\Phi^T = \iint_T U_t ds \cong \iint_T \sum_k \alpha_k \bar{\lambda}_k . \bar{r}_k ds = A_T \sum_k \alpha_k \bar{\lambda}_k . \bar{r}_k \qquad (8)$$

With A_T the area of cell *T*. the appropriate constant values $\bar{\lambda}_k . \bar{r}_k$ are derived by requiring discrete conservation

$$\iint_T \left(\bar{F} + \bar{G} \right) ds = \iint_T \left(A\left(\bar{U}\right) U_x + B\left(\bar{U}\right) U_y \right) ds \qquad (9)$$

A condition which leads to choice $\bar{U} = U\left(\bar{Z}\right)$ with $\bar{Z}$ the arithmetic average of the Roe parameter vector at each node of the triangle (details are available in [1] for example).

$$\bar{Z} = \left(Z_1 + Z_2 + Z_3\right)/3 \qquad (10)$$

$$Z_i = \sqrt{\rho_i}\left[1 \quad u_i \quad v_i \quad H_i\right]^T / 3, \quad i = 1,2,3 \qquad (11)$$

The flow field values at a given node *i* may be updated in time by assembling contributions from all of the triangles sharing the node T_i. Integration of (5) over the median dual cell control volume D (fig.1) gives

$$\iint_D U_t ds = \sum_i \iint_{T_i} U_t ds = -\sum_i \beta^{T_i} \Phi^{T_i} \qquad (12)$$

The coefficients β^{T_i} determine how much of the fluctuation from cell T_i is sent to node *i* and are chosen so as to implement upwinding. Usually this is done separately for each eigenmode so we also attach a *k* index to the distribution coefficients, $\beta_k^{T_i}$. From the above we may construct the first order time integration scheme:

$$U_i\left(t + \Delta t\right) = U_i\left(t\right) - \frac{\Delta t}{A_D} \sum_i \left(A_{T_i} \sum_k \beta_k^{T_i} \alpha_k \bar{\lambda}_k \bar{r}_k \right) \qquad (13)$$

With A_D the area of the median dual cell control volume. Higher order time advancement is possible but we shall be mainly concerned with using time integration as means to compute a final steady state, usually employing local time stepping, so (13) is sufficient.

Each member of the class of numerical schemes defined by (13) is defined by:

1- A choice of the eigenmodes used in the expansion of the cell gradients (6). This is called the wave model.

2- A choice of the coefficients $\beta_k^{T_i}$. This is called the distribution scheme.

Fluctuation distribution schemes have a number of attractive theoretical and practical properties:

The wave model may determine the directions $\vec{\mu}_k$ dynamically during a computation. This is in contrast to many conventional schemes in which the directions along which the Jacobian $\vec{F^U}$ is projected are fixed usually they are the normals to the cell edges. Use of the cell normals leads to a grid dependence of the solution and a misinterpretation of gradients which are not aligned with the cell edge normals [8]. Dynamic computation of the directions $\vec{\mu}_k$ significantly reduces grid dependence.

The computational stencil is narrow, limited to one cell. This is very advantageous in parallelization of the code and also eliminates the need for memory space for storing node adjacency information.

The above presentation employed the conservation variable *U* as typically used in a computer code. For the purposes of theoretical analysis it is more convenient to use the primitive variables $V=[\rho \;\; u \;\; v \;\; p]^T$ due the simpler form of the Jacobian $\vec{F}^V = A^V \vec{i} + B^V \vec{j}$ and eigenvectors.

$$A^V = \begin{bmatrix} u & \rho & 0 & 0 \\ 0 & u & 0 & 1/\rho \\ 0 & 0 & u & 0 \\ 0 & \rho c^2 & 0 & u \end{bmatrix}, \quad B^V = \begin{bmatrix} v & 0 & 1/\rho & 0 \\ 0 & v & 0 & 0 \\ 0 & 0 & v & 1/\rho \\ 0 & 0 & \rho c^2 & v \end{bmatrix} \tag{14}$$

$$r^{a\pm} = \begin{bmatrix} \rho \\ \pm c\cos\theta^a \\ \pm c\sin\theta^a \\ \rho c^2 \end{bmatrix}, \; r^s = \begin{bmatrix} 0 \\ -c\sin\theta^s \\ c\cos\theta^s \\ 0 \end{bmatrix}, \; r^e = \begin{bmatrix} \rho \\ 0 \\ 0 \\ 0 \end{bmatrix} \tag{15}$$

The above eigenvectors correspond to the acoustic, shear and entropy modes respectively, and are associated with the eigenvalues: $\lambda^{a\pm} = \vec{\mu}^a \cdot \vec{V} \pm c$, $\lambda^s = \vec{\mu}^s \cdot \vec{V}$, $\lambda^e = \vec{\mu}^e \cdot \vec{V}$.

3. METHODS

3.1. The original Roe wave models

For any given triangle *T* the gradient $\vec{\nabla} V$ has 8 components in 2D. There are therefore "8" degrees of freedom in choosing a wave model. These may be any combination of wave strengths α_k and wave orientations $\vec{\mu}_k(\theta_k)$. The first wave models proposed by Roe (for a complete presentation, see [11]) used six eignenmodes: 4 acoustic oriented along directions θ^a, $\theta^a+\pi/2$, $\theta^a+\pi$, $\theta^a+3\pi/2$, 1 entropy wave oriented along θ^e and 1 shear wave oriented along θ^s. The angles θ^e, θ^s are determined dynamically for each cell at each time step. The non-linear system (6) admits an exact analytic solution [11].

$$\begin{cases} \theta^e = \tan^{-1} \dfrac{\rho_y - \dfrac{p_y}{\rho c^2}}{\rho_x - \dfrac{p_x}{\rho c^2}} \sqrt{\left(\rho_x - p_x/\rho c^2\right)^2 + \left(\rho_y - p_y/\rho c^2\right)^2} \\ \alpha^e = \end{cases} \tag{16}$$

$$\alpha^s = \left(v_x - u_y\right)/c, \quad \theta^a = \frac{1}{2}\tan^{-1}\frac{v_x + u_y - c\alpha^s\cos(2\theta^s)}{u_x - v_y + c\alpha^s\sin(2\theta^s)} \tag{17}$$

$$\begin{cases} \alpha^{a^1} + \alpha^{a^2} = \left(u_x + v_y\right)/c + R \\ \alpha^{a^1} - \alpha^{a^2} = \left(p_x\cos\theta^a + p_y\sin\theta^a\right)/\rho c^2 \end{cases} \tag{18}$$

$$\begin{cases} \alpha^{a3} + \alpha^{a4} = \left(u_x + v_y\right)/c - R \\ \alpha^{a3} - \alpha^{a4} = \left(p_y\cos\theta^a - p_x\sin\theta^a\right)/\rho c^2 \end{cases} \tag{19}$$

Where: $$R=\sqrt{\left[\frac{\left(v_x+u_y\right)}{c}-\alpha^s\cos 2\theta^s\right]^2+\left[\frac{\left(u_x+v_y\right)}{c}+\alpha^s\sin 2\theta^s\right]^2} \quad (20)$$

The angle θ^s has to be imposed. Different choices determine different variants of the original Roe six-wave models:

i) Wave Model B proposed by Roe [7]: θ^s is chosen perpendicular to the flow direction. In this model, the shear does not provide a contribution to the cell fluctuation.

ii) Wave Model C of De Palma et al. [14]: θ^s is chosen aligned along the pressure gradient. This model has problems in recognizing isolated shear layers through which pressure is constant.

iii) Wave Model D of Roe [13]: It is based on the strain-rate axes and couples the shear and acoustic wave fronts in the following form,

$$\theta^s=\theta^a+\pi/4\,\mathrm{sgn}\left(v_x-u_y\right) \quad (21)$$

This model produces acoustic waves aligned with the principal strain-rate tensor.

3.2. Linear distribution schemes

The choice of a wave model determines the α_k coefficients in (13), i.e. the fluctuation. In order to completely define the numerical scheme one must also specify how the cell fluctuation is distributed to the nodes. In the distribution stage upwinding is applied to each wave mode. There exist two classes of relative position of the wave vector $\vec{\mu}_k$ with respect to triangle: either there is only one downstream node in which case the wave mode is said to be single-target or there are two downstream nodes in which case the wave mode is said to be two-target. In the single-target case the entire fluctuation is sent to the downstream nodes. In the two-target case the fluctuation must be somehow apportioned between the two downstream nodes. There are many distribution schemes available (see [7] for an extensive presentation) differing only in how they treat the two-target case. A general classification which is important in establishing numerical accuracy is with respect to the dependence of the scheme coefficients upon the field values. Equation (13) may be formally rewritten as $U_i\left(t+\Delta t\right)=\sum_j a_j U_j$, if the coefficients a_j do not depend on the nodal values the scheme is said to be linear. If we have $a_j=a_j\left(U\right)$ the scheme is non-linear. We shall consider just two of the most widely used linear schemes. We shall assume node 1 is upstream and nodes 2 and 3 are downstream. See figure 2.

3.2.1. The N scheme

Uses a distribution based upon decomposing the wave vector along the cell edges:

$$\vec{\mu}_k=\vec{\mu}_{k,2}+\vec{\mu}_{k,3} \quad (22)$$

This lead to the distribution coefficients:

$$\beta_2=\vec{\mu}_{k,2}\cdot\vec{\mu}_k,\quad \beta_3=\vec{\mu}_{k,3}\cdot\vec{\mu}_k \quad (23)$$

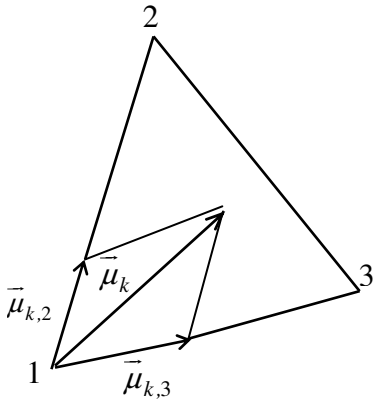

FIGURE 2: The geometric interpretation of the N scheme

3.2.2. The LDA scheme

Uses a distribution based upon the areas delimited by the wave vector

$$\beta_2 = A_2/A_T\,, \quad \beta_3 = A_3/A_T \tag{24}$$

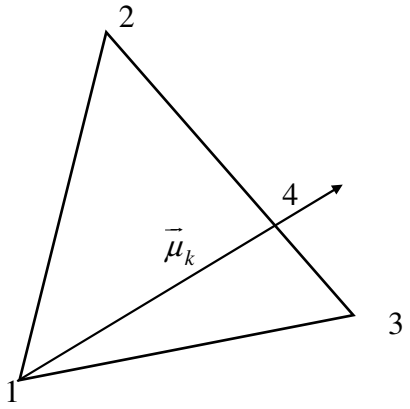

FIGURE 3: The geometric interpretation of the LDA scheme

3.3. Non-linear distribution schemes

The above linear distribution schemes are first order accurate in space which is not sufficient for practical work. Sidilkover [9] showed how to obtain second order accuracy by using limiter functions. Limiters are applied only in the two-target case. The general form of a limited fluctuation distribution is :

$$\Phi_{2,\lim} = \Phi_2 - L\left(\Phi_2 - \Phi_3\right),\ \Phi_{3,\lim} = \Phi_3 - L\left(\Phi_2 - \Phi_3\right) \tag{25}$$

With the limiter function satisfying the properties of (1) linearity preservation L(a, a) = a and (2) symmetry L(a, b) = L(b, a).
Common limiter functions are:

- **MinMod:** $$L(a,\ b) = sgn(a)\,max\left[0,\ min\left(|a|,\ sgn(a)\,b\right)\right] \tag{26}$$

- **Harmonique:** $$L(a,\ b) = \frac{1}{2}\left(1 + sgn(ab)\right)\frac{2ab}{a+b} \tag{27}$$

- Superbee:
$$L(a,\ b)=\frac{1}{2}(1+sgn(\ ab\ ))\,b\,max\left[\ min\left(\frac{2a}{b},1\right),\ min\left(\frac{a}{b},2\right)\right] \quad (28)$$

4. Computational examples and Results

The test cases presented in this paper have been chosen specifically to show the performance of our Code in capturing oblique shock. All cases analyzed were run on unstructured triangular grids type Delaunay-Voronoï, the generator of mesh is called Emc2 developed at the Laboratory Jacques-Louis Lions, University of Pierre et Marie Curie in Paris.
For all the aerodynamic test cases presented in this paper the flow is from left to right and is initially set to take the freestream values throughout the domain.

For all illustrations, we show the iso-Mach lines of the steady state solutions using **Roe's Model "D"** with the minmod limiter. The five test cases studied are:

4.1. Supersonic Oblique Shock Reflection

The first test case is designed to exhibit the shock capturing capabilities of the scheme in supersonic flow.

The domain defined by (x, y) $\in$ [0,4] $\times$ [0,1]. The grid for this domain is shown in the Fig.4.

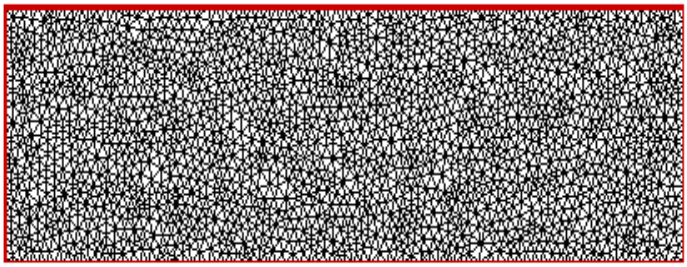

FIGURE 4: The grid for the oblique shock reflection test case.

The boundary conditions are set so that an oblique shock enters the domain with an incoming Mach number of 2.5 at the top left hand corner at an angle of 29° to the horizontal, is reflected by a flat plate along the lower boundary, approximately 45% of the distance along the channel and leaves the domain again just below the top right hand corner, figure 5.

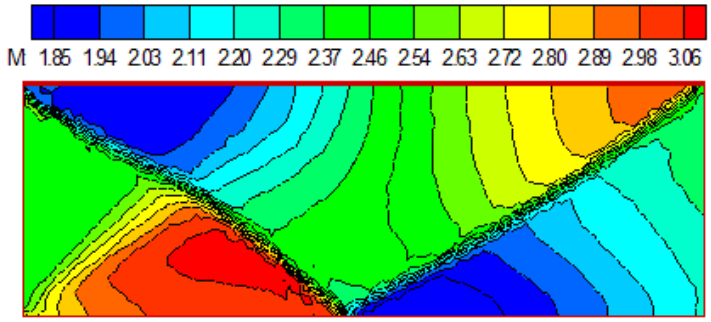

FIGURE 5: Mach contours for the oblique shock reflection.

4.2. Flow in a Channel with a Bump

In this second test case we consider the two regimes:

4.2.1. Transonic flow: The flow is over a domain defined by (x, y) ∈ [0,3] × [0,1] and with 10% circular arc bump, the Mach number is M_∞ = 0.675. The grid for this domain is shown in the Figure 6.

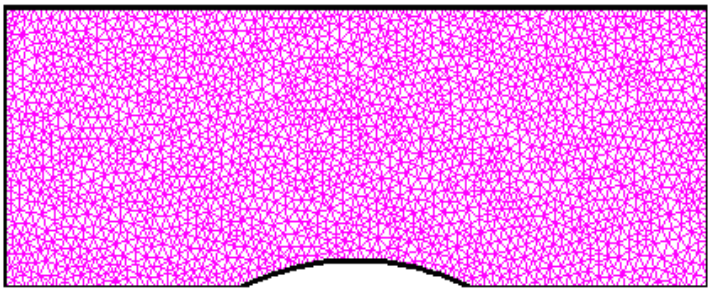

FIGURE 6: The grid for the constricted channel with a 10% circular arc bump on the lower surface.

The resulting flow contains a single shock on the lower surface, about 72% downstream along the bump, figure 7.

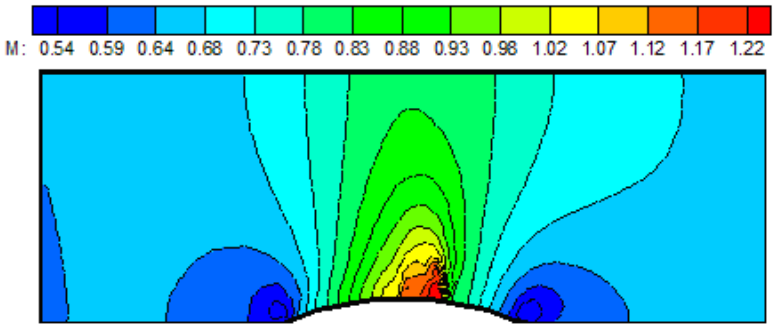

FIGURE 7: Mach contours in a Channel with a Bump, M_∞ = 0.675, 10% circular arc bump.

4.2.2. Supersonic flow: The flow is over a 4% circular arc bump, Mach number is M_∞ = 1.4. The steady state flow is completely supersonic with strong shocks being created at both the front and rear of the bump which are reflected of the walls of the channel further downstream, see figure 8.

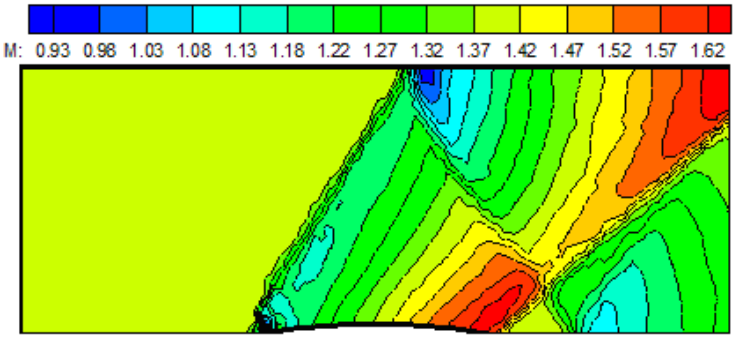

FIGURE 8: Mach contours in a Channel with a Bump, M_∞ = 1,4 and 4% circular arc bump.

4.3. Symmetric Constricted channel flows "Cosine bump channel"

In the third test case the computational domain represents a channel of length 3 meters and width 1 meter, with bumps of the same shape and size in the centre of either wall of the channel. The bumps are one meter in length and are defined such that the breadth of the channel is given by:

$$B = B_0 - 2B_h \cos^2\left(\frac{x - x_c}{x_l} \cdot \pi\right) \quad \text{for } |x - x_c| \le \frac{x_l}{2}, \qquad (29)$$

Where:
B_0=1 is the breadth of the channel.
B_h is the height of each bump, in this case is taken to be 0.04.
x_c=1.5 is the x coordinate of the center of the constriction.
X_l=1 is the length of each bump.

The grid, shown in Figure 9 contains 2631 nodes and 5050 triangular cells.

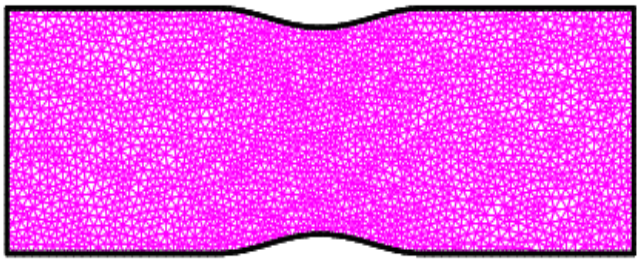

FIGURE 9: The grid for the symmetric constricted channel flow test cases.

4.3.1. Subsonic case:

The inflow Mach number is given as M_∞ = 0,5, the resulting steady solution is a subsonic, isentropic, symmetric solution about the bump, see figure 10.
The boundary conditions are: the upper and lower surfaces are solid walls, and characteristic conditions are applied at the subsonic inlet and outlet.

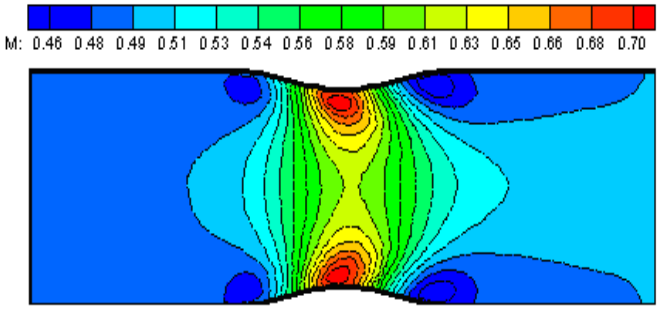

FIGURE 10: The grid for the symmetric constricted channel flow test cases.

4.3.2. Transonic case:

In this case we consider Mach number is M_∞ = 0.71.
We remark the appearance of a band of shock downstream from the two arcs which gives a normal shock wave, see figure 11.

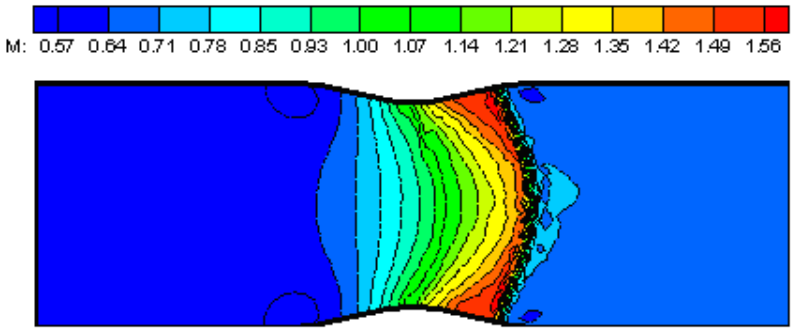

FIGURE 11: The grid for the symmetric constricted channel flow test cases.

4.3.3. Supersonic case:

In this case we consider Mach number is M_∞=1.6.
The result of the flow in this case is the shock waves appeared upstream and downstream from the two bumps.

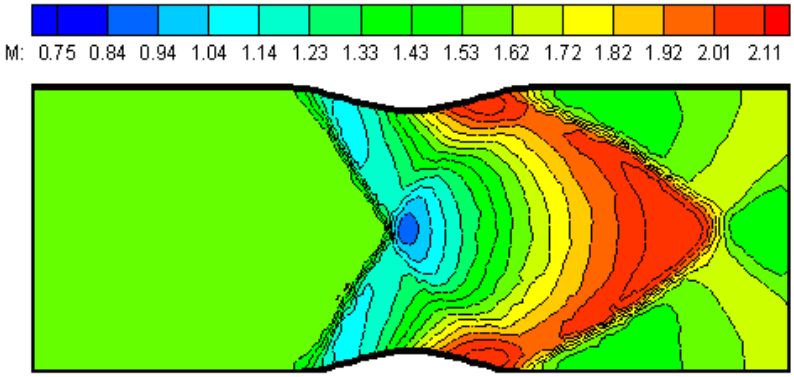

FIGURE 12: The grid for the symmetric constricted channel flow test cases.

4.4. NACA0012 Aerofoil

The third test case present the two dimensional flow around a symmetric NACA0012 aerofoil which is the most common geometries used by aerodynamicists to validate CFD codes because experimental and numerical results are available for a wide variety of flow speeds and angles of incidence.

We consider two problems, transonic and supersonic flows. The grid consists of 260 nodes on the aerofoil, the far field boundary has been located at 30 chords distance, giving a total of 6137 nodes. The complete grid is shown in figure 13 and the region close to the aerofoil is shown in figure 14. The boundary conditions imposed are a solid wall tangency condition on the surface of the airfoil; with the freestream values plus a vortex correction imposed at the far field boundary.

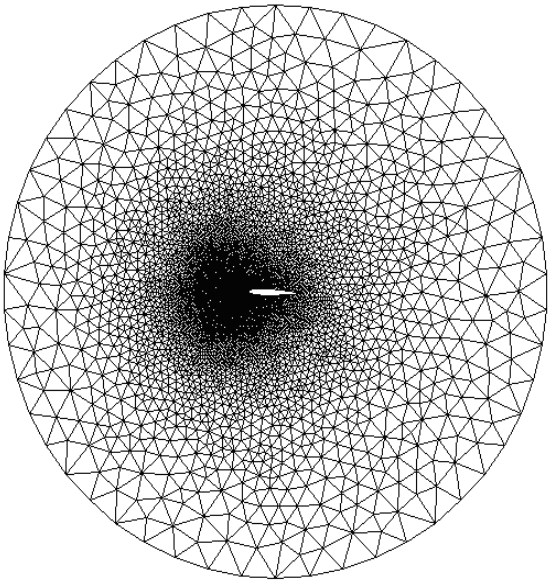

FIGURE 13: Grid around the NACA 0012 aerofoil.

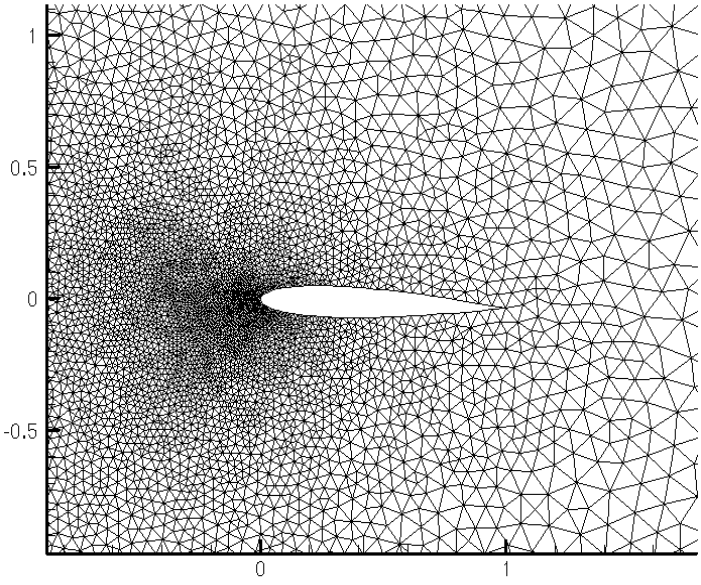

FIGURE 14: Details of NACA 0012 grid.

4.4.1. Transonic flow: We take the Mach number to be $M_\infty = 0.85$ and an angle of attack of $\alpha = 1°$. We notice the appearance of a strong shock near the tail of the aerofoil on the upper surface and a slightly weaker shock further upstream on the lower surface, figure 15.

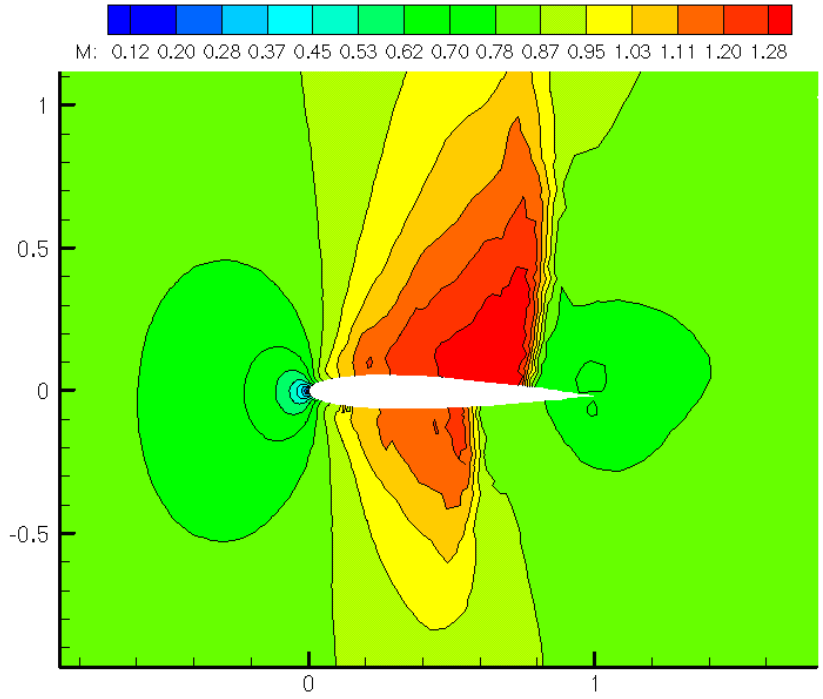

FIGURE 15: Transonic flow over NACA 0012, $M_\infty = 0.85$, $\alpha = 1°$; Mach contours.

4.4.2. Supersonic flow: Mach number is $M_\infty = 1.2$, $\alpha = 0°$. The solution shown in the figure 16 shows the capacity of the code to capture the shock waves, then a shock wave detached upstream from the profile, what is in conformity with the results obtained in the literature.

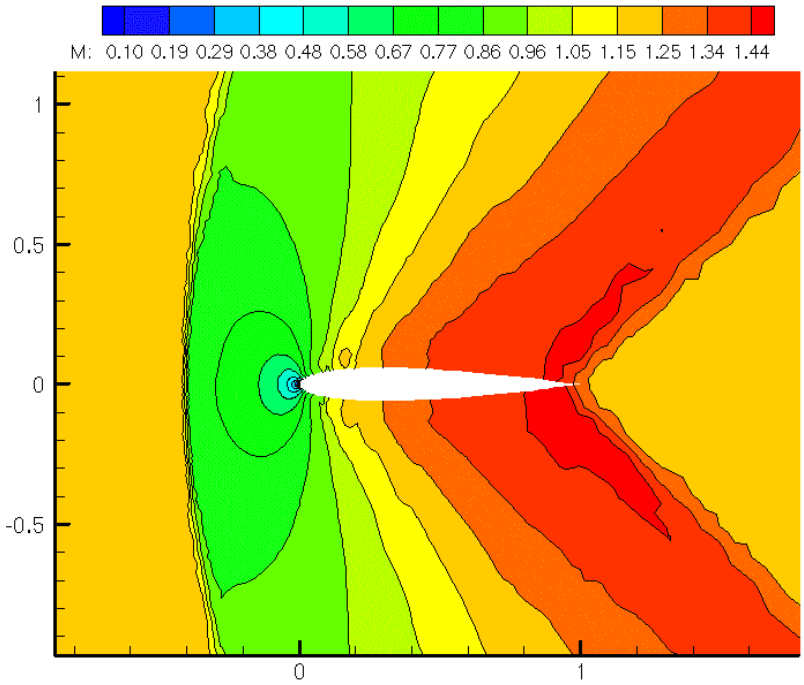

FIGURE 16: Supersonic flow over NACA 0012, $M_\infty = 1.2$, $\alpha = 0°$; Mach contours.

4.5. VKI-59 Turbine Cascade

The last test case is that of a transonic flow through the VKI LS-59 gas turbine cascade which has been measured on wind tunnels and computed by many researchers. In our case, at the inlet boundary the flow angle is 30°, total pressure and total temperature are set to 1bar and 293 K. A static back pressure of 0.407 bar, which is equal to an isentropic Mach number of 0.85. The Mach contours of the transonic flow through turbine cascade VKI LS-59 is shown in figure 18.

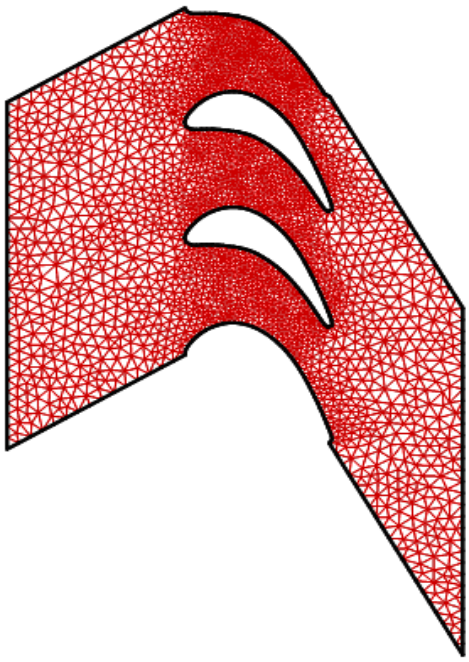

FIGURE 17: The grid for the Transonic flow through turbine cascade VKI LS-59.

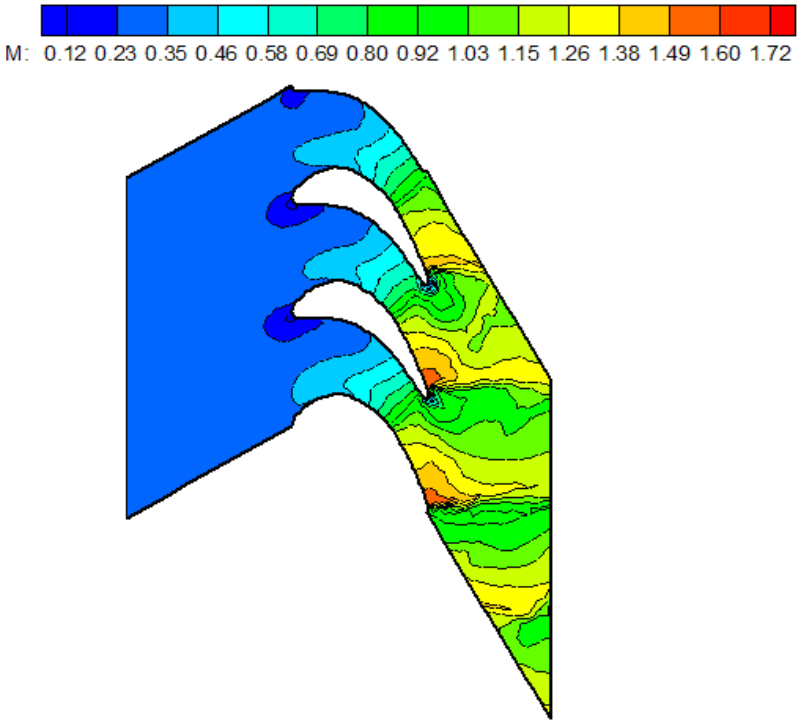

FIGURE 18: Transonic flow through turbine cascade VKI LS-59; Mach contours.

5. CONCLUSION & FUTURE WORK

The aim of this work is achieved, for each of the test cases the original Roe wave model type D is applied (which decompose the Euler equations into a set of six simple wave equations). When this model is combined with the fluctuation splitting N scheme it gives a very robust method for solving the Euler equations in complex geometries.

The purpose of the numerical results reported in our work show that our code written in C++ is comparable in accuracy, efficiency and robustness to others.

The ability of the code to capture the shock waves in different regimes: subsonic, transonic and supersonic flows has been illustrated, our results in all test cases are comparable with those produced in the literature.

In the future, we intend to study the efficiency of multidimensional upwind methods for the solution of conservation laws by applying grid adaptation (Effect of mesh refinement and the movement of nodes).

Acknowledgments

The authors would like to thank members of the "Laboratory Jacques-Louis Lions, University of Pierre et Marie Curie" in Paris, who provided the authors with the software Emc2: is a portable, interactive and graphic software Edition of two dimensional geometry and mesh generator.

REFERENCES

1. PL. Roe. *"Approximate Riemann solvers, parameter vectors and difference schemes"*. J. Computational Physics. 43(2):357-372, 1981.

2. H. Deconinck, R. Struijs, G. Bourgois, PL. Roe. *"High resolution shock capturing cell vertex advection schemes for unstructured grids"*. Lecture series, Van Kareman Institute for fluid dynamics. 5: H1-H79,1994.

3. H. Deconinck, R. Struijs, G. Bourgois, H. Paillere, PL. Roe. *"Multidimensional upwind methods for unstructured grids*. In AGARD, Special Course on Unstructured Grid Methods for Advection Dominated Flows. N92-27671 18-34, 1992.

4. H. Deconinck, PL., Roe, R. Struijs. *"A multidimensional generalization of roe's flux difference splitter for the Euler equations"*. Journal of Computers Fluids. 22:215-222, 1993.

5. R. Struijs, H. Deconinck, P. De Palma, PL. Roe, KG. Powell. *"Progress on multidimensional upwind Euler solvers for unstructured grids"*. In Computational Fluid Dynamics Conference, 10th, Honolulu, HI, June 24-26, 1991.

6. H. Paillere, H. Deconinck, E. Van der Weide. "Upwind residual distribution methods for compressible flow". In 28th CFD Lecture Series, Bruxelles, VKI for Fluid Dynamics, 1997.

7. PL. Roe. *"Discrete models for the numerical analysis of time-dependent multidimensional gas dynamics"*. Journal of Computational Physics, 43:458-476, 1986.

8. PL. Roe. *"Algorithmic trends in CFD, chapter Beyond the Riemann Problem"*. Springer-Verlag, Part I, 341-367, 1993.

9. D. Sidilkover, PL. Roe. *"Unifaction of some advection schemes in two dimensions"*. Technical report, ICASE, TR-95-10, 1995.

10. ME. Hubbard. *"Multidimensional Upwinding and grid adaptation for conservation Laws"*. PhD Thesis, University of Reading, 1996.

11. L. Mesaros. *"Multi-Dimensional Fluctuation Schemes for the Euler Equations on Unstructured Grids"*. PhD Thesis, University of Michigan,1995.

12. N. Venkatakrishnan. *"A Perspective on Unstructured Grid Flow Solvers"*. ICASE Report 95-3, 1995.

13. PL. Roe, L. Mesaros. *"An improved wave model for the multi-dimensional upwinding of the Euler equations"*. In Proceedings of the Thirteenth International Conference on Numerical Methods in Fluid Dynamics, Rome, July 1992.

14. P. De Palma, H. Deconinck and R. Struijs. *"Investigation of Roe's 2D wave decomposition models for the Euler equations"*. Technical report, Von Karman Institute for Fluid Dynamics, TN-172, June 1990.

15 B. Laskarzewska and M. Mehrvar. *"Atmospheric Chemistry in Existing Air Atmospheric Dispersion Models and Their Applications*: Trends, Advances and Future in Urban Areas in Ontario, Canada and in Other Areas of the World*"*. International Journal of Engineering (IJE), Volume (3) : Issue (1), 2009.

16 R. Atan, A. A. A. Ghani, M. Selamat and R. Mahmod.*"Automating Measurement for Software Process Models using Attribute Grammar Rules"*. International Journal of Engineering (IJE), Volume (1) : Issue (2), 2007.

17 S. Manchanda, M. Dave and S. B. Singh. *"Genetic Information System Development and Maintenance Model For Effective Software Maintenance and Reuse"*. International Journal of Engineering (IJE), Volume (1) : Issue (1), 2007.